PERGAMON

International Journal of Heat and Mass Transfer 44 (2001) 2555–2565

International Journal of HEAT and MASS TRANSFER

www.elsevier.com/locate/ijhmt

Choked flow of low density gas in a narrow parallel-plate channel with adiabatic walls

W. Shi, M. Miyamoto *, Y. Katoh, J. Kurima

Department of Mechanical Engineering, Yamaguchi University, Tokiwadai 2-16-1, Ube, Yamaguchi 755-8611, Japan

Received 10 November 1999; received in revised form 16 June 2000

Abstract

The continuum and slip choked flows of low-density air through a narrow parallel-plate channel with adiabatic walls are investigated by means of finite-difference numerical calculation, experiment and analytical solution. In the numerical calculation based on two-dimensional compressible viscous boundary layer equations, the previous method is improved to achieve a higher precision of the choked state by decoupling the pressure term from momentum equation. The numerical results of discharge coefficient, pressure distribution and surface temperature distribution agree well with the experimental data. As the upstream tank pressure drops, the numerical results of friction coefficient and recovery factor approach the asymptotic values for the incompressible developed flow.

1. Introduction

The study of flow and temperature fields of rarefied gas in a narrow channel is often encountered in the application of vacuum engineering such as the leak detection of the zinc physical vapor deposition line [1,2]. In the latest decade, with the development of micro-machine technology in such areas as microelectronics, bioengineering and advanced energy systems [3], the studies on slightly rarefied gas flow in micro-channel (i.e. micro-flow) have been carried out by researchers in the fields of micro-electro-mechanical systems (MEMS). In the recent investigations of micro-flow, the effects of gas compressibility, rarefaction and friction have become the major investigation focuses. Especially, the relatively low speed flow or isothermal flow in the micron size channel have been well studied [4,5]. For example, Harley et al. [6] have conducted theoretical analysis and experiments on the gas flow in the micro-parallel-plate channel. The analysis is based on one-dimensional compressible viscous flow equations including the slip effect at channel wall. Although many discussions about the frictional coefficient have been made, the choked flow is just simply referred.

It is well known that the rarefaction effect depends on the Knudsen number, i.e. the ratio of the molecular mean free path to the representative dimension of the channel. As Arkilic et al. [4] pointed out, the study of micro-flow is driven by the study of low density gas in normal-size channel. For the micro-flow, there remains many difficulties in [7]:

- The accurate measurement of mass flow rate.
- The measurement of the pressure and temperature distribution along the channel.
- The characterization of the size and shape of micro-channels.

Nagayama et al. [8] have conducted a two-dimensional calculation of rarefied gas flow with pressure from 6.7 kPa to 0.067 Pa in a 10-cm high channel by the direct simulation Monte Carlo (DSMC) method, and the heat flux of the uniform-temperature wall has also been evaluated. But they have only investigated the flows of velocity lower than 50 m/s and Kn higher than 0.01.

Based on the compressible viscous laminar boundary layer equations, Kashiwagi et al. [9] have conducted a two-dimensional numerical calculation of the critical air

* Corresponding author. Tel.: +81-836-85-9106; fax: +81-836-85-9101.

E-mail addresses: shiwei68@hotmail.com (W. Shi), miyamoto@po.cc.yamaguchi-u.ac.jp (M. Miyamoto).

0017-9310/01/$ - see front matter
PII: S0017-9310(00)00289-1

Nomenclature

a	acoustic velocity
C_d	discharge coefficient, ratio of actual mass flow rate to that of one-dimensional isentropic flow
C_f	$8\tau_w/(\rho_m u_m^2)$ friction coefficient
C_p	specific heat under constant pressure
G	$\int_0^h \rho u \, dy/(\rho_{00} a_{00} h)$ non-dimensional mass flow rate
h	channel height
k	thermal conductivity
Kn	λ/h or $(0.5\pi\gamma)^{0.5}\, Ma/Re$ Knudsen number
l	channel length
Ma	Mach number
p	pressure
P	p/p_{00} non-dimensional pressure
Pr	$C_p\mu/k$ Prandtl number
q	heat flux
R	gas constant
Re	$Re_{00} = \rho_{00} a_{00} h/\mu_{00}$, $Re_0 = \rho_0 u_0 2h/\mu_0$, Reynolds number
T	temperature
u	x-component of velocity
v	y-component of velocity
x, y	spatial coordinates, see Fig. 1
Xc	$l/(Re_{00} Pr_{00} h)$ non-dimensional nozzle characteristic number

Greek symbols

α	energy accommodation coefficient
γ	ratio of specific heats
λ	molecular mean free path
μ	viscosity
ρ	density
σ	tangential momentum accommodation coefficient
τ_w	$\tau_w = \mu(\partial u/\partial y)_{y=0}$, shear stress of fluid at wall

Subscripts

0	channel inlet
00	upstream tank (stagnant state)
e	channel exit
e0	downstream tank
i, j	grid numbers in x- and y-directions
s	slip flow
w	channel wall surface
m	average across channel
∞	channel centerline, at $y = h/2$

flow in a parallel-plate nozzle with the adiabatic walls or uniform temperature walls. They have compared the numerical results of mean Nusselt number and streamwise gas density distribution with the experimental data [10]. However, their calculations and experiments are just limited to the continuum flow of relatively high upstream tank pressure (i.e. high Reynolds number) which is close to the atmospheric pressure. In either study, field of vacuum engineering or MEMS, the investigations on the choked rarefied gas flow in a parallel-plate channel are still quite limited.

In order to investigate the slightly rarefied gas choke flow in continuum and slip flow region, we generate the rarefaction with low-density gas in a millimeter-size channel. In our previous studies [1,2], an one-dimensional approximation method has been proposed for the continuum and slip flow in a parallel plate channel. The discharge coefficient correlation proposed agrees well with the experimental data for the channels or nozzles with adiabatic walls.

In the present study, in order to compute the flow at the pressure as low as possible using the two-dimensional compressible viscous laminar boundary layer equations, we first improve the iteration method of Kashiwagi et al. [9] by decoupling the pressure term from the momentum equation. With a relatively higher choke precision, the numerical calculations are conducted in a wide range of upstream tank pressure (i.e. Reynolds number). In the experiment, the mass flow rates and wall surface temperature distributions along the channel are measured. A good agreement between the numerical results and the available experimental data is achieved. In addition, an one-dimensional analytical expression of the recovery factor is deduced for the fully developed incompressible internal flow with the velocity slip and temperature jump.

2. Mathematical formulation

2.1. Governing equations

For the continuum and slip gas flow in a narrow parallel-plate channel, the numerical calculation can be based upon the two-dimensional compressible viscous laminar boundary layer equations. The geometry of channel, the Cartesian coordinates and the differential meshes are schematically shown in Fig. 1.

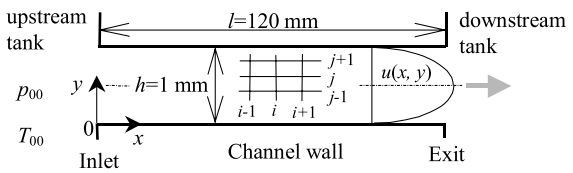

Fig. 1. Two-dimensional parallel-plate channel.

The steady-state governing equations consist of continuity, momentum, energy, and ideal gas state equations:

$$\frac{\partial}{\partial x}(\rho u)+\frac{\partial}{\partial y}(\rho v)=0, \tag{1}$$

$$\rho\left(u\frac{\partial u}{\partial x}+v\frac{\partial u}{\partial y}\right)=-\frac{\mathrm{d}p}{\mathrm{d}x}+\frac{\partial}{\partial y}\left(\mu\frac{\partial u}{\partial y}\right), \tag{2}$$

$$\rho C_{\mathrm{p}}\left(u\frac{\partial T}{\partial x}+v\frac{\partial T}{\partial y}\right)=u\frac{\mathrm{d}p}{\mathrm{d}x}+\frac{\partial}{\partial y}\left(k\frac{\partial T}{\partial y}\right)+\mu\left(\frac{\partial u}{\partial y}\right)^2, \tag{3}$$

$$p=\rho RT. \tag{4}$$

The expressions of mass flow rate, viscosity and thermal conductivity of air are given by:

$$\int_0^h \rho u\,\mathrm{d}y=\rho_0 u_0 h, \tag{5}$$

$$\mu=\mu_{00}(T/T_{00})^{0.76}, \tag{6}$$

$$k=k_{00}(T/T_{00})^{0.86}. \tag{7}$$

2.2. Boundary conditions

In the calculation, all the variables are assumed to be uniformly distributed at the channel inlet of $x=0$. They are evaluated by the assumption of isentropic flow from upstream tank to channel inlet.

For the slip flow, the velocity and temperature boundary conditions are given as follows. Here, due to the channel symmetry about $y=h/2$, only the boundary conditions for $x>0$ and $y=0$ are shown. The velocity boundary conditions are that the vertical velocity v vanishes at the solid wall, and the stream-wise velocity u at wall (i.e. slip velocity) becomes non-zero [11]

$$u_{y=0}\equiv u_{\mathrm{s}}=\frac{2-\sigma}{\sigma}\lambda\left(\frac{\partial u}{\partial y}\right)_{y=0}+\frac{3}{4}\frac{\mu}{\rho T}\left(\frac{\partial T}{\partial x}\right)_{y=0}. \tag{8}$$

Another effect of slip flow is that there exists a temperature jump [11] between the wall surface temperature T_{w} and the contiguous gas temperature $T_{y=0}$

$$T_{\mathrm{w}}=T_{y=0}-\frac{2-\alpha}{\alpha}\frac{2\gamma}{\gamma+1}\frac{\lambda}{Pr}\left(\frac{\partial T}{\partial y}\right)_{y=0}+\frac{1}{C_{\mathrm{p}}}\frac{4\gamma}{\gamma+1}\frac{1-\alpha}{\alpha}\frac{\sigma}{1-\sigma}u_{\mathrm{s}}^2, \tag{9}$$

where $\sigma=1.0$ and $\alpha=0.97$. Here, in the case of continuum flow, Eqs. (8) and (9) become $u_{y=0}=0$ and $T_{\mathrm{w}}=T_{y=0}$, respectively, and the equations from (1)–(9) become just the same as that of Kashiwagi et al. [9].

As Maslen [12] proposed, moreover, the heat transferred to the wall should take into account of the shear stress work q' done by the slipping fluid adjacent to the wall. This effect can be expressed as the boundary condition of

$$k\left(\frac{\partial T}{\partial y}\right)_{y=0}=-q_{\mathrm{w}}-q'=-q_{\mathrm{w}}-\mu u_{\mathrm{s}}\left(\frac{\partial u}{\partial y}\right)_{y=0}, \tag{10}$$

where for adiabatic wall: $q_{\mathrm{w}}=0$, while for continuum flow: $q'=0$. In this numerical calculation, with the drop of upstream tank pressure p_{00} (i.e. the increase of the rarefaction), the continuum boundary conditions are converted to slip ones [7] from $Kn_0\geqq 10^{-3}$. This is equivalent to $p_{00}\leqq 6.69$ kPa for the channel shown in Fig. 2.

Here, some explanations about the boundary condition equation (10) are given. If the energy equation (3) is integrated about y from $y=0$ to $h/2$, the following one-dimensional energy equilibrium equation for slip flow can be obtained:

$$\frac{\mathrm{d}}{\mathrm{d}x}\left(\int_0^{h/2}\rho u\left(\frac{u^2}{2}+C_{\mathrm{p}}T\right)\mathrm{d}y\right)=-\mu u_{\mathrm{s}}\left(\frac{\partial u}{\partial y}\right)_{y=0}-k\left(\frac{\partial T}{\partial y}\right)_{y=0}. \tag{11}$$

It is easy to find that the integral of the left-hand side indicates the total energy brought by the fluid through the channel. Based on the principle of energy conservation, the left-hand side must be equal to the energy conducted through the wall to the fluid q_{w}. Therefore, it is proved that the shear stress work q' should be included in the heat transfer boundary condition for slip flow.

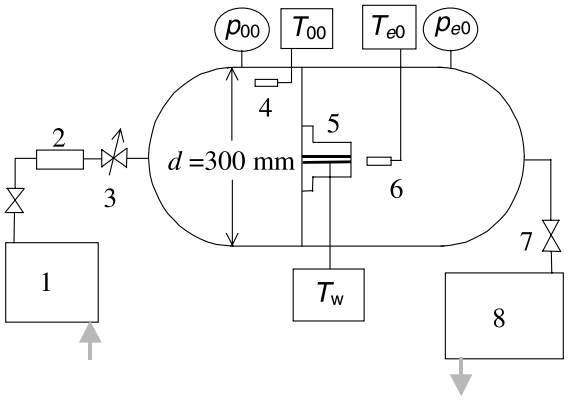

1: Clean-Air System
2: Mass Flow Meter
3: Pressure Regulator
4: Total Temperature Probe
5: Parallel-plate Channel
6: Total Temperature Probe
7: Valve
8: Vacuum Pump System

Fig. 2. Experimental setup.

2.3. Numerical procedure

In the numerical calculation of boundary layer equations, the finite difference forward-marching procedure has the advantages of less computer memory demand and shorter computing time cost. This procedure is first proposed by Bodoia et al. [13] for the viscous incompressible flow in a parallel-plate channel. Kashiwagi et al. [9] have applied it to the compressible flow. In the numerical procedure reported by Miyatake et al. [14], which is commonly used for incompressible flow, the technique of decoupling the pressure term from momentum equation has been adopted for the incompressible flow. With the aim to improve the precision and capability of Kashiwagi's procedure [9] for the low density gas flow, Miyatake's iteration scheme [14] is used in the present computation. In addition, the same discretization scheme as that of Kashiwagi et al. [9] is chosen for the governing equations (i.e. upwind differentiation for the convection term), only besides that Miyatake's [14] discretization methods are employed in the continuity equation and temperature boundary condition. In the non-dimensionalization of the variables in the above governing equations and boundary conditions, the similar manner as that of Kashiwagi et al. [9] is chosen.

The above calculations of each forward-marching step are processed from the channel inlet towards the exit. In order to achieve the choked flow state, the whole-channel calculation is iterated with the assumed inlet velocity u_0 increased gradually until the choke condition of $-\partial G/\partial P_e \leqq e_c$ is satisfied for the given value of p_{00} and T_{00}. Here, e_c is the precision for choked flow state.

3. Experimental setup and method

The experimental setup is schematically depicted in Fig. 2. From the clean-air system 1 (composed of a compressor, a dryer and two filters), the air passes through the mass flow meter 2, pressure regulator 3 and then flows into the vacuum tank. The vacuum tank with the diameter of 300 mm is separated into two chambers by a flange on which the test section 5 is installed. The air is finally exhausted into the vacuum pump system 8. The pressure-regulated air in the upstream tank is approximately at the room temperature.

In the measurement of mass flow rate, five types of laminar air flow meter (precision: <2.5%) are used for different ranges of p_{00}. For the cases of $p_{00} \leqq 0.17$ kPa, the capacitance manometer with unsteady method (precision: <0.15%) is employed. In this method, the mass flow rate is calculated based on the rising speed of p_{e0} after the valve 7 is closed while p_{00} remains constant. For the flow in choked state, p_{00} can be kept constant for several seconds if p_{e0} is low enough. At this moment, the capacitance manometer with high time-responsibility is employed in the measurement of p_{e0} variation. In the measurements of steady pressures, the digital manometers and Mcleod gauge are used.

The channel walls (19.0-mm thick) are made of paper-base phenolic resin with a glossy and smooth surface (maximum roughness $R_{max} = 0.88$ μm). As shown in Fig. 1, the channel is 1.0-mm high, 120-mm long and 50.5-mm wide. Two inner surfaces of the channel are plated with 1-μm(±10%) thick Nickel. They are supplied with DC to generate an uniform heat flux in the later experiments. This plating technology can keep the surface roughness almost the same as that before plating. The wall surface temperatures at 10 locations with different values of x are measured by the Type-E thermocouples with the diameter of 25 μm. Each thermocouple is embedded just beneath the surface. The distance of each thermocouple junction to the channel inner surface is less than 0.5 mm. In order to confirm the adiabatic effect of wall, a point of the channel outer surface temperature is also measured.

4. Results and discussions

4.1. Choked state and discharge coefficient

Under certain upstream tank pressure, as the downstream tank pressure drops down, the mass flow rate through the channel increases gradually to a saturation value, which is termed as the choked state. As Kashiwagi et al. [9] studied, however, it is not easy to obtain the choked state in two-dimensional calculation as exactly as that in one-dimensional approximate solution. It has also been shown in the experimental study [15] that the lower the upstream tank pressure becomes, the more difficult the choked state can be achieved.

In the flow range of $1000 \geqq 1/Xc \geqq 5.05$, Kashiwagi et al. [9] approximately calculated the choked continuum flow with a choke precision of $e_c = 1\%$. Here, Xc is the nozzle characteristic number proposed by Kashiwagi et al. [9]. In the continuum flow model of this study, a higher choke precision and a wider applicable region ($1000 \geqq 1/Xc \geqq 1.87$) are obtained than those of Kashiwagi et al. [9]. The calculated examples of the choke precision e_c achieved in the present study are shown in Table 1, as well as the value of relative choke precision $e_c \times P_e/G$ and the pressure of upstream tank and channel exit. As shown in this table, for all the cases when $p_{00} > 1.36$ kPa, the choke precision values are approved to be lower than 1% of Kashiwagi et al. [9]. When the upstream tank pressure p_{00} becomes lower, it tends to be difficult to obtain a small value of the choke precision e_c. When $p_{00} < 1.36$ kPa, the maximum Mach number at the channel exit cannot exceed 1 so that the deviation

Table 1
Precision for choked flow state

$1/Xc$	P_{00} (kPa)	P_e (kPa)	e_c (%)	$e_c \times P_e/G$ (%)	$\Delta x/(hRe_{00}) \times 10^{-5}$[a]	$\Delta y/h \times 10^{-2}$
12.91	9.4	2.0	0.05	0.04	0.95	2.0
3.68	2.7	0.3	0.05	0.046	8.5	1.25
1.87	1.36	0.18	0.31	0.552	8.5	1.25
0.75	0.55	0.11	1.5	9.2	8.5	1.25

[a] For $x/l \leqslant 0.05$ or $x/l \geqslant 0.95$.

from the choked state seems to become large, especially near the channel exit. In addition, $e_c \times P_e/G$ can be considered to be a more reasonable criterion than e_c for the low-density gas flow, because it can take into account of the extreme reduction of mass flow rate when the pressure is very low. This value is smaller than 0.552% when $p_{00} > 1.36$ kPa.

In order to make a comparison, Fig. 3 shows the discharge coefficients C_d of this numerical results by the continuum flow model, and that of Kashiwagi's numerical results [9], as well as the analytical solution by Eq. (12)

$$C_d = \frac{1}{19.444 Pr_{00}} \frac{1}{Xc} = \frac{0.07176}{Xc}. \tag{12}$$

Eq. (12) derived from Arkilic et al. [4] gives the limiting value for the isothermal flow in a very long channel ($l \to \infty$) with extremely low pressure ratio ($p_e/p_{00} \to 0$). It is corresponding to the solution of $C_f \times Re_0 = 96$ in the following.

In Fig. 3, the numerical results of Kashiwagi et al. [9] are re-plotted in the dash line (the values are read from their figure). As the pressure p_{00} decreases, the numerical results of this study become higher than their results, with the maximum about 10% higher at $1/Xc = 5.05$. As p_{00} reduces further, the discharge coefficient of this calculation asymptotically approaches to the isothermal flow value predicted by Eq. (12).

If the slip boundary conditions are applied in the calculation, the choke precision obtained can be smaller than that by the continuum model. This will be confirmed by the comparisons between the experimental data and calculated results in next section. As shown in Fig. 5, when p_{00} is as low as about 0.32 kPa ($1/Xc = 0.42$), this slip model can still give almost the same discharge coefficient as that of the experimental data or one-dimensional approximation result. As indicated in Fig. 6, moreover, the stream-wise pressure distributions predicted by this slip model agree well with the experimental data even at $1/Xc = 0.628$. In the subsequent parts of this paper, the comparisons and discussions of the numerical results and experimental data are made for the flow regime of $p_{00} \geqq 0.32$ kPa ($1/Xc \geqq 0.42$). In this flow regime, the relative choke precision of $-(\partial G/\partial P_e) \times P_e/G$ is less than 8%, and the value of local Knudsen number is lower than 0.06.

In order to clearly illustrate the previously mentioned choke precision by some examples, Fig. 4 shows the variations of dimensionless mass flow rate G with drop of the downstream tank pressure p_{e0}, while the upstream

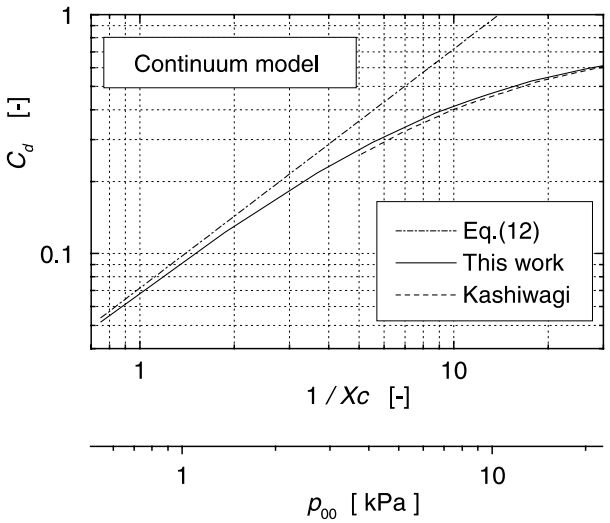

Fig. 3. Application range of continuum model.

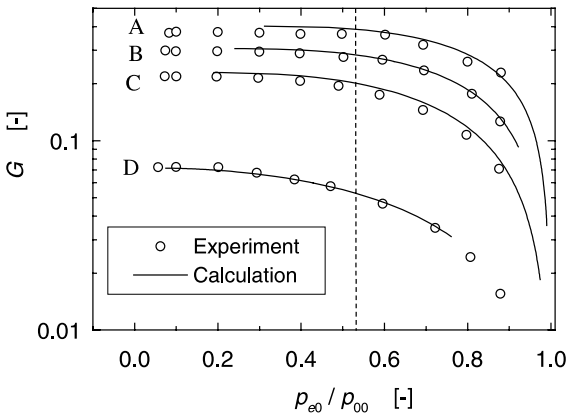

	p_{00} [kPa]	Kn_0	Ma_0	Re_0	$1/Xc$
A:	40.0	0.00019	0.455	7477.7	55.35
B:	13.35	0.00053	0.326	1822.8	17.49
C:	6.65	0.00104	0.237	690.6	8.75
D:	1.32	0.00514	0.072	41.5	1.73

Fig. 4. Camparison of the choked flow state.

tank pressure p_{00} keeps constant. Here, in the numerical data, the channel-exit pressure p_e is employed as the downstream tank pressure p_{e0}, because this calculation is just conducted from the upstream tank to the channel exit. It is shown that the numerical results are in a good agreement with the experimental data. In both experiment and calculation, as p_{00} drops down, the minimum value of pressure ratio p_{e0}/p_{00} for achieving the choked state tends to be far smaller than 0.528 of the isentropic flow. This may be mainly attributed to the viscous effect in both experiment and numerical calculation.

4.2. Discharge coefficient

Fig. 5 shows the two-dimensional numerical calculation and one-dimensional approximation [1] results of the discharge coefficient, as well as the experimental data. For the slip model, almost the same results of C_d are given by this two-dimensional calculation as that by one-dimensional analysis. A good agreement is obtained between the numerical results and the experimental data. For p_{00} higher than about 13.3 kPa, the numerical values of C_d appears to be slightly higher than the experimental data, which implies that the flow may have developed into the turbulent flow. In the low pressure region of $p_{00} \leqq 0.13$ kPa, the scatter of the experimental values becomes apparent. At $p_{00} = 0.08$ kPa, this two-dimensional slip model gives too low value and appears not applicable due to the high Knudsen number which is close to the transition flow region.

4.3. Distributions of pressure and friction coefficient

Because the measurement of the stream-wise pressure distribution has not been conducted in this experiment, the experimental data ($h = 0.7$ mm, $l = 150$ mm) of our previous study [2] are plotted in Fig. 6 to compare with the numerical results. Fig. 6 shows a good agreement between them for both continuum flow of $p_{00} = 13.33$ kPa and slip flow of $p_{00} = 1.33$ kPa.

For the isothermal continuum flow in a very long channel, the pressure distribution expression of Eq. (13) can be obtained from the analysis of Arkilic et al. [4], and also shown in Fig. 6.

$$\frac{p}{p_{00}} = \sqrt{1 - \frac{x}{l}}. \tag{13}$$

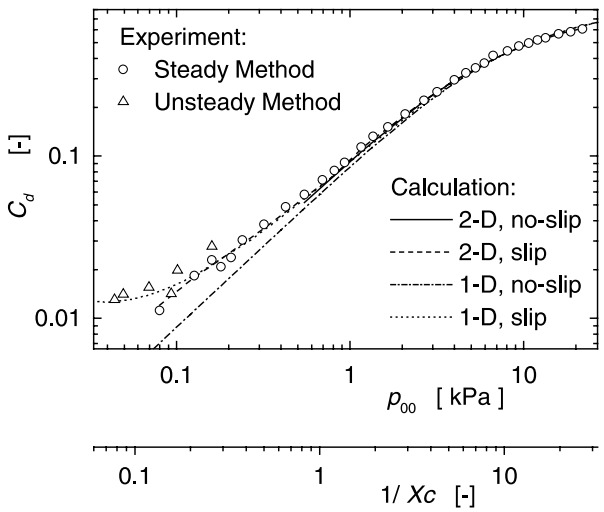

Fig. 5. Discharge coefficient C_d.

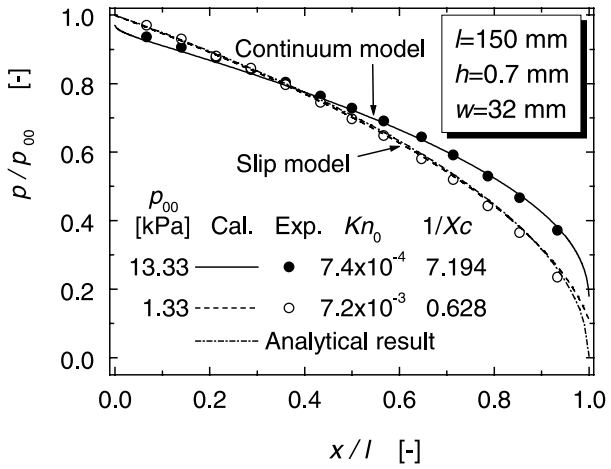

Fig. 6. Comparison of pressure distribution.

It can be clearly found in Fig. 6 that, except the vicinity of channel exit, the analytical solution given by Eq. (13) is only in a good agreement with the two-dimensional numerical result in the case of $p_{00} = 1.33$ kPa. In this case, the numerical value of Kn_∞ increases from 7.2×10^{-3} at the inlet to 5.0×10^{-2} at the exit.

Fig. 7 shows the distributions of the friction coefficient in the form of $C_f \times Re_0$ for several typical cases of this numerical calculation. In the cases of higher p_{00}, the frictional loss appears quite large in the vicinity of channel inlet and exit. With the drop of p_{00}, these inlet/exit effects tend to diminish, and the overall distribution tends to drop to the value of the fully developed incompressible flow. In the cases of $p_{00} \leqq 1.36$ kPa, due to the relatively high rarefaction the distributions become lower than the value of $C_f \times Re_0 = 96$.

4.4. Distributions of wall surface temperature and recovery factor

It is well known that the wall surface temperature of adiabatic flow is very important in the heat transfer analysis of high-speed compressible flow. The adiabatic wall temperature has been well studied in the boundary layer flow on a flat plate, and is usually correlated with the recovery factor r. It has become a common knowledge that for laminar flow: $r = Pr^{1/2}$; while for turbulent flow: $r = Pr^{1/3}$. However, investigations on adiabatic wall temperature for the internal flow are very few. McAdams et al. [16] have measured the adiabatic wall temperature for the subsonic turbulent flow in a pipe, and pointed out that it is rational to define the heat transfer coefficient with the adiabatic wall temperature. Although Kashiwagi et al. [9] have discussed the heat

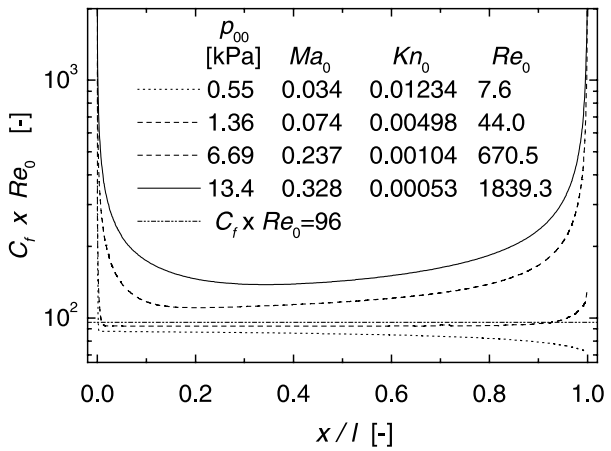

Fig. 7. Fricition coefficient distribution.

transfer characteristics for the uniform-temperature wall, they have not presented either numerical or experimental results of the adiabatic wall temperature. Whereas in the research field of MEMS [5], some efforts have been paid on the development of the surface temperature sensor for micro-channel, but the experimental results have not been reported yet.

In this study, the stream-wise adiabatic wall temperature distribution has not only been calculated but also measured for a wide range of pressure. In Fig. 8(a), the numerical results at $p_{00} = 2.67$, 4.0, 8.09 kPa are compared with the experimental data. The numerical results are in relatively good agreement with the experimental data at $p_{00} = 2.67$ kPa. As the p_{00} increases, however, the nearer to the channel exit the lower the numerical results are than the experimental data. At $p_{00} = 8.09$ kPa ($Re_0 = 916.2$) the maximum absolute temperature difference is about 1.5 K at $x/l = 0.917$.

In the experiment, the wall surface temperature distribution has the tendency to be uniform along the channel length due to the heat conduction in the wall so that the absolute adiabatic wall condition is hard to be satisfied. On the other hand, however, because the conductivity of the paper-base phenolic resin wall is so small ($k \fallingdotseq 0.23$ W/m^2 K)), it seems that this temperature difference cannot be attributed to the heat conduction in wall only. The possibility that the flow may have developed into the turbulent flow should not be excluded [17,18].

In the lower pressure cases of $p_{00} = 1.36$ and 0.55 kPa, the velocity slip and temperature jump at wall become relatively significant. As shown in Fig. 8(b), the numerical results given by the slip model with the shear stress work q' incorporated, are compared with the results by that q' ignored. The measured wall surface temperatures appear to be uniformly distributed along the channel, and the numerical results with q' incorporated give the distributions much closer to the experimental data.

Moreover, in order to investigate the variation of adiabatic wall temperature for a wider range of p_{00}, the experimental and numerical results of ΔT ($= T_w - T_{00}$)

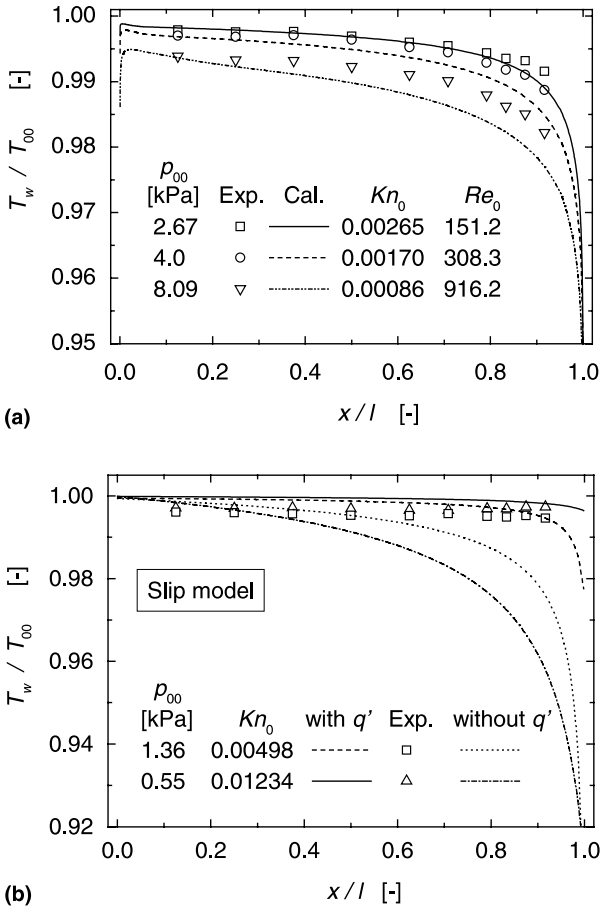

Fig. 8. Channel wall surface temperature distributions.

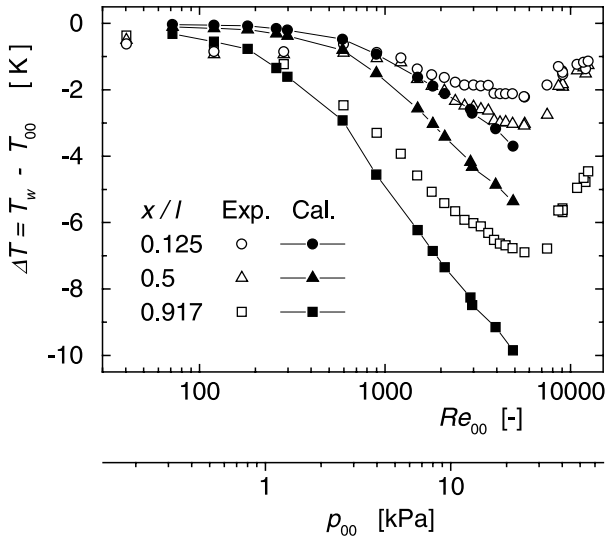

Fig. 9. Surface temperature variation with p_{00}.

at the positions of $x/l = 0.125$, 0.5 and 0.917 are shown in Fig. 9. For p_{00} lower than about 0.32 kPa, both numerical and experimental values of ΔT appear to be constant and close to zero. As p_{00} rises, the absolute value of ΔT tends to be enlarged gradually, as well as the differences between the experimental data and numerical results. In the region that the flow could be considered as laminar flow ($p_{00} \leqq 8.09$ kPa), the numerical values can well predict the variation of experimental results. At about $p_{00} = 25.3$ kPa, the experimental data of the value of ΔT reaches the minimum at all positions, and then increases as the pressure p_{00} rises up further.

For the internal flow, the recovery factor r is defined by McAdams et al. [16] as follows:

$$r = \frac{T_{\mathrm{aw}} - T_{\mathrm{m}}}{T_{00} - T_{\mathrm{m}}} = \frac{T_{\mathrm{aw}} - T_{\mathrm{m}}}{(u^2)_{\mathrm{m}}/2C_{\mathrm{p}}}, \tag{14}$$

where T_{m} is the bulk mean temperature, and $(u^2)_{\mathrm{m}}/2$ is the kinetic energy carried by the unit mass of the fluid through the channel cross-section.

For the fully developed incompressible flow in a parallel channel with adiabatic walls, the analytical solutions of velocity and temperature can be obtained by integrating Eqs. (2) and (3). By incorporating the first-order velocity slip and temperature jump boundary conditions, the velocity and temperature profiles across the channel can be obtained as:

$$\frac{u}{u_\infty} = \frac{4\psi Kn + 1 - \eta^2}{4\psi Kn + 1}, \tag{15}$$

$$T = T_{\mathrm{w}} - \frac{\eta^4 - 2(4\psi Kn + 1)\eta^2 + 1 + 16\psi Kn + 32\psi\beta Kn^2}{2(4\psi Kn + 1)^2}\frac{Pr}{C_{\mathrm{p}}}u_\infty^2. \tag{16}$$

Here

$$\eta = \frac{y}{h}, \quad \psi = \frac{2-\sigma}{\sigma}, \quad \beta = \frac{2-\alpha}{\alpha}\frac{2\gamma}{\gamma+1}\frac{1}{Pr}.$$

Therefore, the recovery factor r defined by Eq. (14) becomes

$$r = Pr \times \frac{1 + 14\psi Kn + (140/3)(\psi+\beta)\psi Kn^2 + 280\beta\psi^2 Kn^3}{1 + 14\psi Kn + 70(\psi Kn)^2 + 140(\psi Kn)^3}. \tag{17}$$

For the continuum flow when $Kn = 0$, $r = Pr$ and the value of r becomes greater than Pr as Kn increases. This suggests that the recovery factor of the internal continuum flow is smaller than that of the flow on a flat plate if $Pr < 1$. As p_{00} drops from 13.4 to 0.55 kPa (similar to Fig. 7), the numerical distribution of r along channel length tends to rise up and approach $r = Pr$ gradually although it is not plotted here. As shown in Fig. 9, when p_{00} is higher than 25.3 kPa, the measured ΔT increases. This indicates that the value of r is close to 1 in turbulent flow, which is in accordance to the values of $r = 0.875 \sim 0.905$ obtained by McAdams et al. [16] for subsonic turbulent air flow in pipe at atmospheric pressure.

4.5. Distributions of velocity and temperature across channel

In the typical cases of $p_{00} = 13.4$, 6.69, 1.36 kPa, the numerical results of velocity and temperature distributions across the channel are shown in Fig. 10. Meanwhile, the analytical solutions of continuum flow

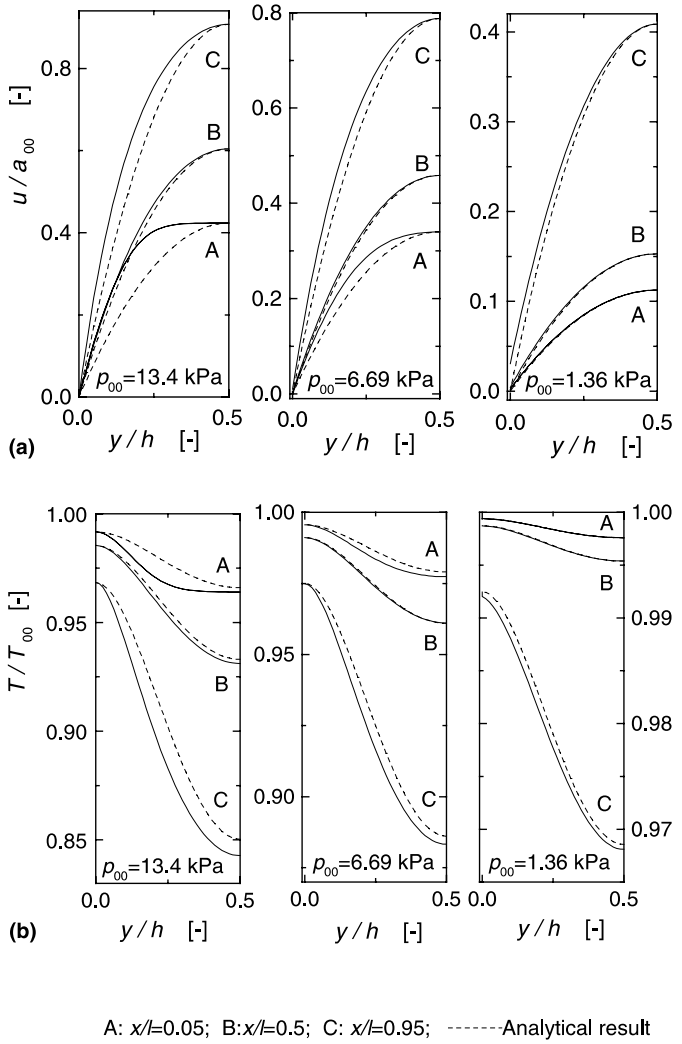

Fig. 10. Velocity and temperature profiles across the channel.

($Kn = 0$) given by Eqs. (15) and (16) are also plotted for a comparison, where the values of velocity u_∞ and temperature T_w are from the two-dimensional numerical results.

As shown in Fig. 10(a), in high-pressure case of $p_{00} = 13.4$ kPa, there remains the potential flow near the channel inlet ($x/l = 0.05$) in the numerical results of velocity distribution. Due to the acceleration of the flow along the channel, even at the middle of the channel ($x/l = 0.5$) there still exists some deviations from the analytical solution of fully developed incompressible continuum flow. This deviation is greatly enlarged near the channel exit ($x/l = 0.95$). In the slip flow of $p_{00} = 1.36$ kPa, the two-dimensional numerical result gives almost the same velocity profile as the analytical one, except some differences caused by the slip velocity at the wall. Therefore, this suggests again that the numerical values tend to be close to the analytical values of incompressible flow with the drop of pressure p_{00} or the increase of rarefaction. Fig. 10(b) shows the similar tendency of the temperature distributions. Also in the case of $p_{00} = 1.36$ kPa, the deviation of the two-dimensional numerical results from the analytical solution in the vicinity of the exit might be attributed to the relatively high temperature jump at the wall and the flow acceleration for the choked state.

5. Conclusions

The characteristics of the velocity and temperature field of choked low-density gas flow in a narrow parallel-channel with adiabatic walls have been clarified by

means of numerical calculation, experiment and analytical approximate solution for a wide range of pressure (Reynolds number) region covering the continuum and slip flow. The main concluding remarks can be summarized as:

1. A two-dimensional numerical method is proposed for choked low-pressure flow including slip flow. It is shown that the numerical results agree well with the available experimental data on discharge coefficient, pressure distribution and wall surface temperature distribution.
2. The characteristic of the friction coefficient distribution along the channel has been quantitatively clarified.
3. From the continuum flow to the slip flow, the adiabatic wall temperature distributions are successfully measured. The effect of shear stress work caused by the slipping fluid at the wall is quantitatively shown. Moreover, it is proved that the temperature recovery factor r of fully developed incompressible laminar internal flow is equal to Pr, which is different from the value of $r = Pr^{1/2}$ of the laminar boundary layer flow on a flat plate.

Acknowledgements

Many of the experimental devices in this research were supported by Dr. Etsuro Hirai, Hiroshima Research Institute of Mitsubishi Heavy Industry Ltd. Here, the authors truly appreciate his kind assistance.

References

[1] T. Taguchi, E. Hirai, M. Kato, M. Miyamoto, Y. Katoh, T. Nagata, Discharge characteristics of low-density gas flow through parallel plate channel with narrow gap, JSME Int. J. Serious B 39 (3) (1996) 470–474.

[2] T. Taguchi, K. Yanagi, M. Miyamoto, T. Nagata, Precise discharge characteristics of rarefied critical flows through a parallel plate channel, in: J. Harvey, G. Lord (Eds.), Rarefied Gas Dynamics, Proceedings of the 19th International Symposium, vol. 1, University of Oxford, 1995, pp. 382–388.

[3] L. O'Connor, MEMS: microelectromechanical systems, Mech. Engrg. 114 (2) (1992) 40–47.

[4] E.B. Arkilic, M.A. Schmidt, K.S. Breuer, Gaseous slip flow in long microchannels, J. Microelectromech. Syst. 6 (2) (1997) 167–178.

[5] K.C. Pong, C.M. Ho, J. Liu, Y.C. Tai, Non-linear pressure distribution in uniform microchannels, Appl. Microfabrication Fluid Mech. ASME, FED 197 (1994) 51–56.

[6] J.C. Harley, Y. Huang, H.H. Bau, J.N. Zemel, Gas flow in micro-channels, J. Fluid Mech. 284 (1995) 257–274.

[7] A. Beskok, G.E. Karniadakis, W. Trimmer, Rarefaction and compressibility effects in gas microflows, Trans. ASME 118 (1996) 448–456.

[8] K. Nagayama, B. Farouk, C.K. Oh, Heat transfer in low pressure (high Knudsen number) developing flows through parallel plates, in: J.S. Lee (Ed.), Heat Transfer 1998, Proceedings of the 11th IHTC, vol. 3, Kyongju, Korea, 1998, pp. 127–132.

[9] T. Kashiwagi, N. Isshiki, Y. Kurosaki, Heat transfer of the critical air flow in a nozzle (1st report: numerical study on heat transfer of the critical air flow in a nozzle with parallel walls), Bull. JSME 22 (163) (1979) 63–70.

[10] N. Isshiki, T. Kashiwagi, Heat transfer of the critical air flow in a nozzle (2nd Report: experimental study on heat transfer of the critical air flow in a nozzle with parallel walls), Bull. JSME 22 (169) (1979) 944–951.

[11] E.M. Sparrow, S.H. Lin, Laminar heat transfer in tubes under slip-flow conditions, J. Heat Transfer, Trans. ASME, November 1962, 363–369.

[12] S.H. Maslen, On heat transfer in slip flow, J. Aeronautical Sci. 25 (1958) 400–401.

[13] J.R. Bodoia, J.F. Osterle, Finite difference analysis of plane poiseuille and couette flow developments, Appl. Sci. Res. A 10 (3-4) (1961) 265–276.

[14] O. Miyatake, T. Fujii, A numerical analysis of natural convective heat transfer between two parallel vertical plates, The Report of Research Institute of Industrial Science of Kyushu University, vol. 55, 1972, pp. 9–25.

[15] M.W. Milligan, Nozzle characteristics in the transition regime between continuum and free molecular flow, AIAA J. 2 (6) (1964) 1088–1092.

[16] W.H. McAdams, L.A. Nicolai, J.H. Keenan, Measurement of recovery factors and coefficient of heat transfer in a tube for subsonic flow of air, Am. Institute Chem. Eng. 42 (1946) 907–925.

[17] P. Wu, W.A. Little, Measurement of friction factors for the flow of gas in very fine channels used for microminiature Joule–Thomson refrigerators, Cryogenics 23 (1983) 273–277.

[18] P. Wu, W.A. Little, Measurement of the heat transfer characteristics of gas flow in fine channel exchangers used for microminiature refrigerators, Cryogenics 24 (1984) 415–420.